



IMPLEMENTING MULTI-SCALE AGRICULTURAL INDICATORS EXPLOITING SENTINELS

VEGETATION FIELD DATA AND PRODUCTION OF GROUND-BASED MAPS:

**“ROSASCO SITE, PAVIA, ITALY”
3RD JULY 2014**

ISSUE I1.00

EC Proposal Reference N° FP7-311766

Actual submission date : October 2014

Start date of project: 01.11.2012

Duration : 40 months

Name of lead partner for this deliverable: EOLAB



Book Captain: Consuelo Latorre (EOLAB)

Contributing Authors: Fernando Camacho (EOLAB)

Mirco Boschetti, Lorenzo Busetto, Francesco Nutini (CNR-IREA)
Giacomo Fontanelli (CNR-IREA), Luigi Ranghetti (UNIPV)

Project co-funded by the European Commission within the Seventh Framework Program (2007-2013)		
Dissemination Level		
PU	Public	X
PP	Restricted to other programme participants (including the Commission Services)	
RE	Restricted to a group specified by the consortium (including the Commission Services)	
CO	Confidential, only for members of the consortium (including the Commission Services)	

DOCUMENT RELEASE SHEET

Book Captain:	C. Latorre	Date: 01.12.2014	Sign. 
Approval:	R. Lacaze	Date: 18.02.2015	Sign. 
Endorsement:	I. Marin-Moreno	Date:	Sign.
Distribution:			

CHANGE RECORD

Issue/Revision	Date	Page(s)	Description of Change	Release
	01.12.2014	All	First Issue	I1.00

TABLE OF CONTENTS

1.	<i>Background of the Document</i>	10
1.1.	Executive Summary	10
1.2.	Portfolio	10
1.3.	Scope and Objectives.....	11
1.4.	Content of the Document	11
1.5.	Related Document.....	12
2.	<i>Introduction</i>	13
3.	<i>Study area</i>	14
3.1.	Location	14
3.2.	Description of The Test Site	15
4.	<i>Ground measurements</i>	16
4.1.	Material and Methods	16
4.2.	Spatial Sampling Scheme	19
4.3.	ground data.....	20
4.3.1.	Data processing	20
4.3.2.	Content of the Ground Dataset	22
4.3.3.	Ancillary information	25
5.	<i>Evaluation of the sampling</i>	26
5.1.	Evaluation Based On NDVI Values.....	26
5.2.	Evaluation Based On Convex Hull: Product Quality Flag.	27
6.	<i>Production of ground-based maps</i>	29
6.1.	Imagery	29
6.2.	The Transfer Function.....	29
6.2.1.	The regression method.....	29
6.2.2.	Band combination	30
6.2.3.	The selected Transfer Function	31
6.3.	The High Resolution Ground Based Maps	32
6.3.1.	Mean Values	34
7.	<i>Conclusions</i>	36
8.	<i>Acknowledgements</i>	37
9.	<i>References</i>	38

LIST OF FIGURES

Figure 1: Location of Rosasco site, Italy.	14
Figure 2: False color composition (RGB: SWIR-NIR-Red) of Landsat-8 TOC Reflectance image over the 5x5 km ² study area (3 rd , July 2014).	14
Figure 3: Land cover types sampled and the location of the ESUs over the Rosasco site. A worldView-2 image for the 14 th of August (RGB true color) is in the background.	15
Figure 4: Examples of the different land cover types in Rosasco site (Italy). a) Soybean, b) Rice, c) Corn e) Poplar.	15
Figure 5: Left side: Distribution of the sampling units (ESUS) over the study area. Right side: DHP Sampling schemes for rice (upper left panel), poplar (upper right panel), soybean (lower left panel) and corn (lower right panel).	19
Figure 6: Digital Hemispherical Photographs acquired in Rosasco site, (Italy) during the intensive campaign of 3 rd - 4 th July 2014. a) Rice, b) Corn, c) Soybean, and d) Poplar.	20
Figure 7: LAIeff values derived from different methods (CEV5.1, CEV6.1 and Miller's formula) as a function of the averaged value. Rosasco site (Italy), 3 rd July, 2014.	21
Figure 8: LAI values derived from different methods as a function of the averaged value. Rosasco site (Italy), 3 rd July, 2014. Left side: CEV5.1, CEV6.1. and Miller's formula. Right side: CEV5.1 and CEV6.1.	21
Figure 9: Intercomparison of the measured biophysical variables. LAI versus FAPAR (Left side) and FAPAR versus FCOVER (Right side). Rosasco site (Italy) 3 rd July, 2014.	22
Figure 10: LAIeff and LAI measurements acquired in Rosasco site, during the campaign of 3 rd of July 2014. Left: Distribution by land cover type. Right: Distribution by ESUs.	23
Figure 11: As in figure 10 for FAPAR (daily integrated values).	23
Figure 12: As in figure 10 for FCOVER.	23
Figure 13: Distribution of the measured biophysical variables over the ESUs. Rosasco site, during the campaign of 3 rd July, 2014.	24
Figure 14: LAI (effective and actual) and NDVI measurements acquired in Rosasco site during the intensive field campaign 3 rd July 2014, distributed by ESUs.	24
Figure 15: Aerosol Optical Depth (AOD) estimation for 550 nm wavelength	25
Figure 16: Comparison of NDVI distribution between ESUs and over the whole image. Field campaign (3 rd July, 2014), Rosasco site (Italy).	26
Figure 17: Convex Hull test over 20x20 km ² and 5x5 km ² areas. Left side: SNRG combination. Right side: SN combination. Clear and dark blue correspond to the pixels belonging to the 'strict' and 'large' convex hulls. Red corresponds to the pixels for which the transfer function behaves as extrapolator. Rosasco - Italy, 3 rd July 2014.	28
Figure 18: Test of multiple regression (TF) applied on different band combinations. Band combinations are given in abscissa (1=G, 2=RED, 3=NIR and 4=SWIR). The weighted root mean square error (RMSE) is presented in red along with the cross-validation RMSE in green. The numbers indicate the number of data used for the robust regression with a weight lower than 0.7 that could be considered as outliers.	30
Figure 19: LAIeff, LAI, FAPAR and FCOVER results for regression on reflectance using 2 and 4 bands combination. Full dots: Weight>0.7. Empty dots: 0<Weight<0.7 crosses.	31
Figure 20: Ground-based LAI maps (20x20 km ²) retrieved on the Rosasco site (Italy), 3 rd July 2014. Left: LAIeff. Right: LAI.	32
Figure 21: Ground-based FAPAR maps (20x20 km ²) retrieved on the Rosasco site (Italy), 3 rd July 2014.	33
Figure 22: Ground-based FCOVER map (20x20 km ²) retrieved on the Rosasco site (Italy), 3 rd July 2014.	33

Figure 23: Ground-based maps (5x5 km²) retrieved on the Rosasco site (Italy), 3rd July 2014..... 34

LIST OF TABLES

<i>Table 1: Coordinates and altitude of the test site (centre).....</i>	<i>14</i>
<i>Table 2: Measurements conducted during the two days of field campaign in Rosasco site (Italy).....</i>	<i>16</i>
<i>Table 3: Cardinality of DHP measurements, globally and for each land cover class in Rosasco site (Italy).</i>	<i>20</i>
<i>Table 4: The Header used to describe ESUs with the ground measurements.</i>	<i>22</i>
<i>Table 55: Percentages over the two areas over the test site of Rosasco (Italy).Convex hull values: 0=extrapolation of TF, 1=strict convex hull and 2=large convex hull).</i>	<i>27</i>
<i>Table 6: Acquisition properties of Landsat-8 data used for retrieving high resolution maps.</i>	<i>29</i>
<i>Table 7: Transfer function applied to the whole site for LAleff, LAI, FAPAR daily integrated and FCOVER. RW for weighted RMSE, and RC for cross-validation RMSE.</i>	<i>31</i>
<i>Table 8: Mean values and standard deviation (STD) of the HR biophysical maps for the selected 3 x 3 km² area at Rosasco site (Italy).</i>	<i>34</i>
<i>Table 9: Content of the dataset.....</i>	<i>35</i>

LIST OF ACRONYMS

CEOS	Committee on Earth Observation Satellite
CEOS LPV	Land Product Validation Subgroup
CNR	<i>Consiglio Nazionale delle Ricerche</i>
DG AGRI	Directorate General for Agriculture and Rural Development
DG RELEX	Directorate General for External Relations (European Commission)
DHP	Digital Hemispheric Photographs
ECV	Essential Climate Variables
EUROSTATS	Directorate General of the European Commission
ERMES	An Earth Observation Model based Rice Information Service
ESU	Elementary Sample Unit
FAPAR	Fraction of Absorbed Photo-synthetically Active Radiation
FAO	Food and Agriculture Organization
FCOVER	Fraction of Vegetation Cover
GCOS	Global Climate Observing System
GEO-GLAM	Global Agricultural Geo- Monitoring Initiative
GIO-GL	GMES Initial Operations - Global Land (GMES)
GCOS	Global Climate Observing System
GMES	Global Monitoring for Environment and Security
GPS	Global Positioning System
IMAGINES	Implementing Multi-scale Agricultural Indicators Exploiting Sentinels
IREA	<i>Istituto per il Rilevamento Elettromagnetico Dell'Ambiente</i>
JECAM	Joint Experiment for Crop Assessment and Monitoring
LAI	Leaf Area Index
LDAS	Land Data Assimilation System
LUT	Look-up-table techniques
PAI	Plant Area Index
PROBA-V	Project for On-Board Autonomy satellite, the V standing for vegetation.
RMSE	Root Mean Square Error
SPOT /VGT	Satellite Pour l'Observation de la Terre / VEGETATION
SLT	SOLar Time
TOC	Top of Canopy Reflectance
USGS	U.S. Geological Survey. Science organization.
UNFCCC	United Nations Framework Convention on Climate Change
UTM	Universal Transverse Mercator coordinates system
VALERI	Validation of Land European Remote sensing Instruments
WGCV	Working Group on Calibration and Validation (CEOS)

1. BACKGROUND OF THE DOCUMENT

1.1. EXECUTIVE SUMMARY

The Copernicus Land Service has been built in the framework of the FP7 geoland2 project, which has set up pre-operational infrastructures. ImagineS intends to ensure the continuity of the innovation and development activities of geoland2 to support the operations of the global land component of the GMES Initial Operation (GIO) phase. In particular, the use of the future Sentinel data in an operational context will be prepared. Moreover, IMAGINES will favor the emergence of new downstream activities dedicated to the monitoring of crop and fodder production.

The main objectives of ImagineS are to (i) improve the retrieval of basic biophysical variables, mainly LAI, FAPAR and the surface albedo, identified as Terrestrial Essential Climate Variables, by merging the information coming from different sensors (PROBA-V and Landsat-8) in view to prepare the use of Sentinel missions data; (ii) develop qualified software able to process multi-sensor data at the global scale on a fully automatic basis; (iii) complement and contribute to the existing or future agricultural services by providing new data streams relying upon an original method to assess the above-ground biomass, based on the assimilation of satellite products in a Land Data Assimilation System (LDAS) in order to monitor the crop/fodder biomass production together with the carbon and water fluxes; (iv) demonstrate the added value of this contribution for a community of users acting at global, European, national, and regional scales.

Further, ImagineS will serve the growing needs of international (e.g. FAO and NGOs), European (e.g. DG AGRI, EUROSTATS, DG RELEX), and national users (e.g. national services in agro-meteorology, ministries, group of producers, traders) on accurate and reliable information for the implementation of the EU Common Agricultural Policy, of the food security policy, for early warning systems, and trading issues. ImagineS will also contribute to the Global Agricultural Geo-Monitoring Initiative (GEO-GLAM) by its original agriculture service which can monitor crop and fodder production together with the carbon and water fluxes and can provide drought indicators, and through links with JECAM (Joint Experiment for Crop Assessment and Monitoring).

1.2. PORTFOLIO

The ImagineS portfolio contains global and regional biophysical variables derived from multi-sensor satellite data, at different spatial resolutions, together with agricultural indicators, including the above-ground biomass, the carbon and water fluxes, and drought indices resulting from the assimilation of the biophysical variables in the Land Data Assimilation System (LDAS).

The production in Near Real Time of the 333m resolution products, at a frequency of 10 days, using PROBA-V data is carried out in the Copernicus Global Land Service. It should start by covering Europe only, and be gradually extended to the whole globe.

Meanwhile, ImagineS will perform in parallel off-line production over demonstration sites outside Europe. The demonstration of high resolution (30m) products (Landsat-8 + PROBA-

V) will be done over demonstration sites of cropland and grassland in contrasting climatic and environmental conditions.

1.3. SCOPE AND OBJECTIVES

The main objective of this document is to describe the field campaign and ground data collected at Rosasco site - Italy and the up-scaling of the ground data to produce ground-based high resolution maps of the following biophysical variable:

- Leaf Area Index (LAI), defined as half of the total developed area of leaves per unit ground surface area (m^2/m^2). We focused on two different LAI quantities (for green elements):
 - The effective LAI (LAI_{eff}) derived from the description of the gap fraction as a function of the view zenith angle. In addition, effective LAI measures derived at 57.5° are also provided in the ground database.
 - The actual LAI (LAI) estimate corrected from the clumping index.
- Fraction of green Vegetation Cover (FCover), defined as the proportion of soil covered by vegetation, derived from the gap fraction between 0 and 10° of view zenith angle.
- Fraction of Absorbed Photosynthetically Active Radiation (FAPAR), which is the fraction of the photosynthetically active radiation (PAR) absorbed by a vegetation canopy. PAR is the solar radiation reaching the canopy in the $0.4\text{--}0.7\ \mu\text{m}$ wavelength region. We focused on the daily integrated FAPAR computed as the black-sky FAPAR integrated over the day. In addition, two other quantities are provided in the ground database: instantaneous 'black-sky' FAPAR at 10:00h SLT, which is the FAPAR under direct illumination conditions at a given solar position and the 'white-sky' FAPAR, which is the FAPAR under diffuse illumination conditions.

1.4. CONTENT OF THE DOCUMENT

This document is structured as follows:

- Chapter 2 provides an introduction to the field experiment.
- Chapter 3 provides the location and description of the site.
- Chapter 4 describes the ground measurements, including material and methods, sampling and data processing.
- Chapter 5 provides an evaluation of the sampling.
- Chapter 6 describes the production of high resolution ground-based maps, and the selected "mean" values for validation.

1.5. RELATED DOCUMENT

ERMES “ImagineS” Field Campaign report (FP7-SPACE 2013-1-Grant n° 606983): Field campaign report of the measurements collected in 2014 over Rosasco site.

2. INTRODUCTION

Validation of remote sensing products is mandatory to guaranty that the satellite products meets the user's requirements. Protocols for validation of global LAI products are already developed in the context of Land Product Validation (LPV) group of the Committee on Earth Observation Satellite (CEOS) for the validation of satellite-derived land products (Fernandes et al., 2014), and recently applied to Copernicus global land products based on SPOT/VGT observation (Camacho et al., 2013). This generic approach is made of 2 major components:

- The indirect validation: including inter-comparison between products as well as evaluation of their temporal and spatial consistency
- The direct validation: comparing satellite products to ground measurements of the corresponding biophysical variables. In the case of low and medium resolution sensors, the main difficulty relies on scaling local ground measurements to the extent corresponding to pixels size. However, the direct validation is limited by the small number of sites, for that reason a main objective of ImagineS is the collection of ground truth data in demonstration sites.

The content of this document is compliant with existing validation guidelines (for direct validation) as proposed by the CEOS LPV group (Morissette et al., 2006); the VALERI project (<http://w3.avignon.inra.fr/valeri/>) and ESA campaigns (Baret and Fernandes, 2012). It therefore follows the general strategy based on a bottom up approach: it starts from the scale of the individual measurements that are aggregated over an elementary sampling unit (ESU) corresponding to a support area consistent with that of the high resolution imagery used for the up-scaling of ground data. Several ESUs are sampled over the site. Radiometric values over a decametric image are also extracted over the ESUs. This will be later used to develop empirical transfer functions for up-scaling the ESU ground measurements (e.g. Martínez et al., 2009). Finally, the high resolution ground based map will be compared with the medium resolution satellite product at the spatial support of the product.

An intensive field campaign to characterize the vegetation biophysical parameters at the Rosasco (Italy) demonstration site was carried out by CNR-IREA (Institute for Electromagnetic Sensing of the Environment) in the context of the FP7 ERMES (an Earth Observation Model Based Rice Information Service) project. The ERMES project aims to develop a prototype of downstream services based on the assimilation of EO and in situ data within crop model (<http://www.ermes-fp7space.eu/>).

Intensive Field Campaign: 3rd - 4th of July 2014.

Teams involved in field collection:

ERMES: M. Boschetti, L. Busetto, F. Nutini, L. Ranghetti

Contact:

IREA-CNR: Mirco Boschetti - boschetti.m@irea.cnr.it

Francesco Nutini - nutini.f@irea.cnr.it

EOLAB: Fernando Camacho - fernando.camacho@eolab.es

3. STUDY AREA

3.1. LOCATION

“Rosasco” site is in the Province of Pavia in the Italian region Lombardy, located about 50 km southwest of Milan and about 45 km west of Pavia (Figure 1). Ground measurements were conducted over selected fields located on the West side of Rosasco.



Figure 1: Location of Rosasco site, Italy.

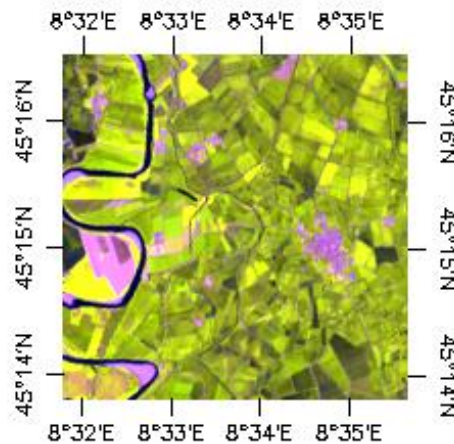


Figure 2: False color composition (RGB: SWIR-NIR-Red) of Landsat-8 TOC Reflectance image over the 5x5 km² study area (3rd, July 2014).

Table 1: Coordinates and altitude of the test site (centre).

Site Center	
Geographic Lat/Ion, WGS-84 (degrees)	Latitude = 45.253° N Longitude = 8.562° E
Altitude	113 m

3.2. DESCRIPTION OF THE TEST SITE

The study area is located between the Sesia river and the city of Rosasco, in Pavia province. Pavia is the capital of a fertile eponymous province known for agricultural products including wine, rice, cereals, and dairy products. The area is located in the main Italian rice district (Figure 3). Other crops present in the area are Soybean, Corn and Poplar plantations (Figure 4). The warmest month of the year is July with an average temperature of 12.3 °C. In January, the average temperature is 1.9 °C. It is the lowest average temperature of the whole year. About 946 mm of precipitation falls annually. There is significant rainfall throughout the year in Rosasco. Even the driest month still has a lot of rainfall.

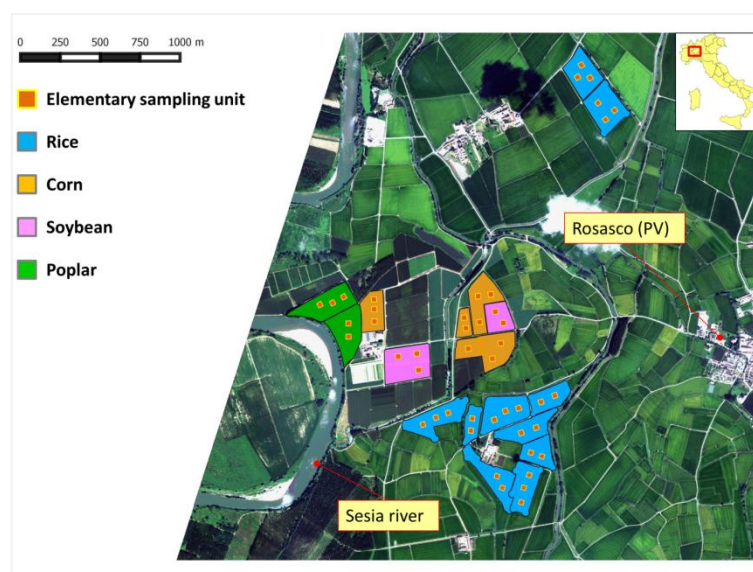


Figure 3: Land cover types sampled and the location of the ESUs over the Rosasco site. A worldView-2 image for the 14th of August (RGB true color) is in the background.



Figure 4: Examples of the different land cover types in Rosasco site (Italy). a) Soybean, b) Rice, c) Corn e) Poplar.

4. GROUND MEASUREMENTS

The ground measurement database reported here was acquired by CNR-IREA.

Table 2 shows the measurements conducted during the field campaign. Digital hemispherical photographs, standard digital photos, plant height and phenological stage were also taken to characterize the fields. Reflectance measurements were taken in 5 fields (Rice and Corn). Sunphotometer measurements for atmospheric correction were taken using an EKO MS-120 sunphotometer with 5 spectral channels. The reflectance measurements were taken over 5 fields (#2 corn, #1 rice and #1 soybean) with a spectrometer (ASD Field Spec FR) in the range of 350-2500nm. In this report, we are focused on the analysis and processing of vegetation biophysical variables.

Table 2: Measurements conducted during the two days of field campaign in Rosasco site (Italy).

Parameters	Measurements	
	Field Campaign (3 rd and 4 th of July, 2014)	
	sampling	cardinality
Digital Hemispherical photos	Every ESU	12-14 per ESU
Standard photos	Every ESU	2 per ESU
Plant height	Every ESU	4 per ESU
Number of leafs/stem	Occasionally	4 per ESU
Reflectance measurements	5 fields	3 transects for fields
Sunphotometer measurements	Concomitant with Landsat-8 overpass	

4.1. MATERIAL AND METHODS

Digital hemispherical photos allow the calculation of LAI, FAPAR and FCOVER measuring gap fraction through an extreme wide-angle camera lens (i.e. 180°) (Weiss et al., 2004). It produces circular images that record the size, shape, and location of gaps, either looking upward from within a canopy or looking downward from above the canopy. Two hemispherical cameras were used during the campaign, both equipped with a full-circle hemispherical lens.

The hemispherical photos acquired during the field campaign were analyzed semi-automatically to compute the biophysical variables. The processing was conducted by the same operator for all the images with the Can Eye software version 6.314 software (developed by INRA <http://www6.paca.inra.fr/can-eye>) to derive LAI, FAPAR daily integrated and FCOVER. It is based on a RGB colour classification of the image to discriminate vegetation elements from background (i.e., gaps). This approach allows exploiting downward-looking photographs for short canopies (background = soil) as well as upward-looking photographs for tall canopies (background = sky). CAN-EYE software processes

simultaneously up to 20 images acquired over the same ESU. Note that our images were acquired with similar illumination conditions to limit the variation of colour dynamics between images.

The processing is achieved in 3 main steps (Weiss et al., 2004). First, image pre-processing is performed, which includes removing undesired objects (e.g. operator, sun glint) and image contrast adjustments to ensure a better visual discrimination between vegetation elements and background. Second, an automatic classification (k-means clustering) is applied to reduce the total number of distinctive colours of the image to 324 which is sufficient to ensure accurate discrimination capacities while keeping a small enough number of colours to be easily manipulated. Finally, a default classification based on predefined colour segmentation is first proposed and then iteratively refined by the user. The allocation of the colours to each class (vegetation elements versus background) is the most critical phase that needs to be interactive because colours depend both on illumination conditions and on canopy elements. At the end of this process a binary image, background versus vegetation elements (including both green and non-green elements) is obtained.

The CAN-EYE software computes biophysical variables from gap fraction as follows:

Effective LAI (LAI_{eff}): Among the several methods described in Weiss et al (2004), the effective LAI estimation in the CAN-EYE software is performed by model inversion. The effective LAI is estimated from the Plant Area Index (PAI) which is the variable estimated by CAN-EYE, as no distinction between leaves or other plant elements are made from the gap fraction estimates. PAI is very close to the effective LAI for croplands when pictures are taken downward looking, whereas larger discrepancies are expected for forest when pictures are taken upward looking. Effective LAI is directly retrieved by inverting Eq. (1) (Poisson model) and assuming an ellipsoidal distribution of the leaf inclination using look-up-table (LUT) techniques.

$$P_0(\theta_v, \varphi_v) = e^{-N \cdot (\theta_v, \varphi_v)} = e^{-G \cdot (\theta_v, \varphi_v) \cdot \frac{LAI_{eff}}{\cos(\theta_v)}} \quad \text{Eq. (1)}$$

A large range of random combinations of LAI (between 0 and 10, step of 0.01) and ALA (Average Leaf Angle) (10° and 80°, step of 2°) values is used to build a database made of the corresponding gap fraction values (Eq.1) in the zenithal directions defined by the CAN-EYE user (60° for the DHP collection in this field campaign). The process consists then in selecting the LUT element in the database that is the closest to the measured P_0 . The distance (cost function C_k) of the k^{th} element of the LUT to the measured gap fraction is computed as the sum of two terms. The first term computes a weighted relative root mean square error between the measured gap fraction and the LUT one. The second term is the regularization term that imposes constraints to improve the PAI estimates. Two equations are proposed for the second “regularization” term:

(1) constraint used in CAN-EYE V5.1 on the retrieved ALA values that assume an average leaf angle close to 60° ± 03°, and

(2) constraint used in CAN-EYE V6.1 on the retrieved PAI value that must be close from the one retrieved from the zenithal ring at 57°. This constraint is more efficient, but it can be computed only when the 57° ring is available (i.e., $\text{COI} \geq 60^\circ$)

The software also proposed other ways of computing PAI and ALA effective using Miller's formula (Miller, 1967) which assumed that gap fraction only depends from view zenith angle. Furthermore, the CAN-EYE makes an estimation using the Welles and Norman (1991) method used in LAI-2000 for 5 rings. These LAI2000-like estimates were not used here as are based on the same Miller's formula but using limited angular sampling.

LAI: The actual LAI that can be measured only with a planimeter with however possible allometric relationships to reduce the sampling, is related to the effective leaf area index through:

$$LAI_{eff} = \lambda_0 \cdot LAI \quad \text{Eq. (2)}$$

where λ_0 is the clumping index. In CAN-EYE, the clumping index is computed using the Lang and Xiang (1986) logarithm gap fraction averaging method, although some uncertainties are associated to this method (Demarez et al., 2008). The principle is based on the assumption that vegetation elements are locally assumed randomly distributed. Values of clumping index given by CAN-EYE are in certain cases correlated with the size of the cells used to divide photographs.

As the CAN-EYE software provides different results (CEV6.1, CEV5.1 and Miller's) for LAI and LAI_{eff} variables; an average LAI value was provided as ground estimate, and the standard deviation of the different considered methods was reported as the uncertainty of the LAI estimate (see associated 20140703_VGM_Rosasco.xls file).

FCOVER is retrieved from gap fraction between 0 to 10°.

$$FCOVER = 1 - P_0 \cdot (0 - 10^\circ) \quad \text{Eq. (3)}$$

FAPAR: As there is little scattering by leaves in that particular spectral domain due to the strong absorbing features of the photosynthetic pigments, FAPAR is often assumed to be equal to FIPAR (Fraction of Intercepted Photosynthetically Active Radiation), and therefore to the gap fraction. The actual FAPAR is the sum of two terms, weighted by the diffuse fraction in the PAR domain: the 'black sky' FAPAR that corresponds to the direct component and the 'white sky' or the diffuse component.

The instantaneous "Black-sky FAPAR" ($FAPAR^{BS}$) is given at a solar position (date, hour and latitude). Depending on latitude, the CAN EYE software computes the solar zenith angle every solar hour during half the day (there is symmetry at 12:00). The instantaneous FAPAR is then approximated at each solar hour as one minus the gap fraction in the corresponding solar zenith angle:

$$FAPAR^{BS}(\theta_s) = 1 - P_0 \cdot (\theta_s) \quad \text{Eq. (4)}$$

The daily integrated black sky or direct FAPAR is computed as the following:

$$FAPAR_{Day}^{BS} = \frac{\int_{\text{sunrise}}^{\text{sunset}} \cos(\theta_S) \cdot [1 - P_0(\theta_S)] \cdot d\theta}{\int_{\text{sunrise}}^{\text{sunset}} \cos(\theta_S) \cdot d\theta} \quad \text{Eq. (5)}$$

In this report we focused on the daily integrated FAPAR, as instantaneous black-sky FAPAR measured at 10:00 was not available for all the ESUs. White-sky FAPAR is also provided in the ground database.

4.2. SPATIAL SAMPLING SCHEME

Downward measurements were conducted on Rice and Soybean. Upward measurements were taken instead on Poplar and Corn.

Four different land cover types (i.e., rice, soybean, corn, poplar) were characterized during the campaign. A pseudo-regular sampling was used within each ESU of approximately 30x30 m². The centre of the ESU was geo-located using a GPS. A total of 43 ESUs were characterized (Table 3). The number of hemispherical photos per ESU ranges between 12 and 15. The 43 ESUs are mainly located over rice fields, that is the main crop in the area. Fields were selected because of the size and the diversity of crop management (e.g. sowing date, cultivar etc.) as reported and mentioned in a session with the farmers. Downward measurements were conducted on Rice and Soybean. Upward measurements were taken instead on Poplar and Corn.

The sampling scheme for the DHP collection is shown in Figure 5 (see also Figure 3). The ground measurements are spread across fields of Corn, Rice, Soybean and Poplar.

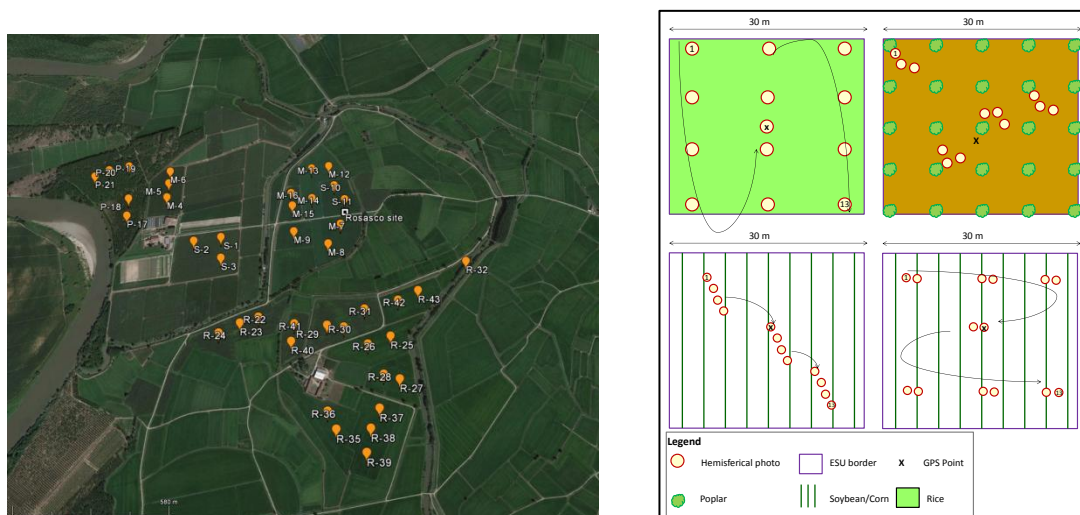


Figure 5: Left side: Distribution of the sampling units (ESUS) over the study area. Right side: DHP Sampling schemes for rice (upper left panel), poplar (upper right panel), soybean (lower left panel) and corn (lower right panel).

Table 3 summarizes the number of fields, sampling units (ESUs) and DHPs collected per each crop type acquired during the field campaigns.

Table 3: Cardinality of DHP measurements, globally and for each land cover class in Rosasco site (Italy).

ESU internal code	Number of ESU's		
	Field Campaign (3 rd and 4 th of July, 2014)		
	N° fields	N° ESUs	N° DHPs
Poplar	2	5	60
Corn	4	11	132
Soybean	2	5	60
Rice	9	22	286
Total	17	43	538

4.3. GROUND DATA

4.3.1. Data processing

The software CAN-EYE version V6.314 was used to process the DHP images. Figure 6 shows some examples of DHP over different land cover types.

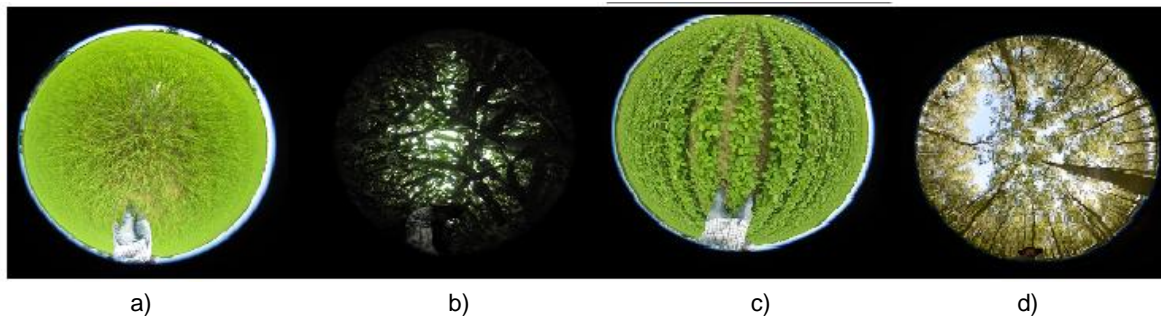


Figure 6: Digital Hemispherical Photographs acquired in Rosasco site, (Italy) during the intensive campaign of 3rd- 4th July 2014. a) Rice, b) Corn, c) Soybean, and d) Poplar.

Effective LAI values were calculated with the average of three different estimations (CEV6.1, CEV5.1 and Miller's) as described in Section 4.1. These estimations were found very consistent for the effective LAI (Figure 7), and the averaged value was used for determining the empirical transfer function. However, for the actual LAI values, large dispersion was found between CEV6.1 or CEV5.1 and Miller's method. As the Miller's method only uses

zenithal angles, we have computed an averaged LAI value using the two estimates based on the Can-Eye approaches (Figure 8).

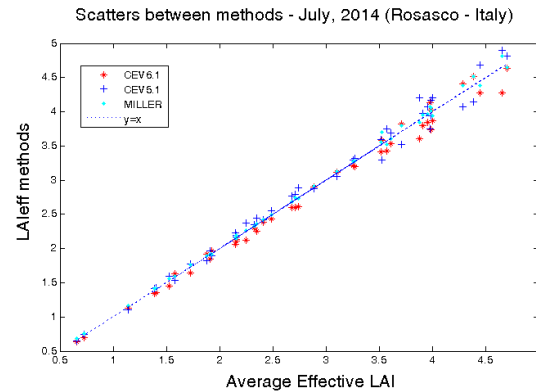


Figure 7: LAIeff values derived from different methods (CEV5.1, CEV6.1 and Miller's formula) as a function of the averaged value. Rosasco site (Italy), 3rd July, 2014.

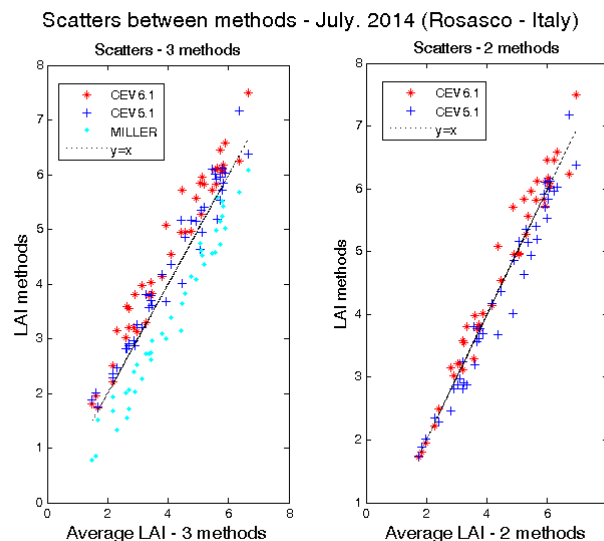


Figure 8: LAI values derived from different methods as a function of the averaged value. Rosasco site (Italy), 3rd July, 2014. Left side: CEV5.1, CEV6.1. and Miller's formula. Right side: CEV5.1 and CEV6.1.

Figure 9 shows the intercomparison between LAI and LAIeff with FAPAR daily estimates, and between FAPAR and FCover. As can be observed, the relationship between variables follows the expected exponential trend between LAI and FAPAR, and the linear trend between FCover and FAPAR.

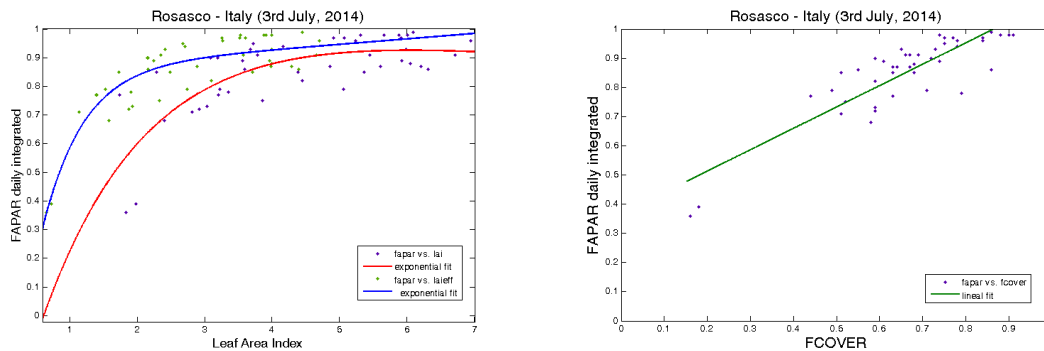


Figure 9: Intercomparison of the measured biophysical variables. LAI versus FAPAR (Left side) and FAPAR versus FCOVER (Right side). Rosasco site (Italy) 3rd July, 2014.

4.3.2. Content of the Ground Dataset

Each ESU is described according to a standard format. The header of the database is shown in Table 4.

Table 4: The Header used to describe ESUs with the ground measurements.

Column	Var.Name		Comment
1	Plot #		Number of the field plot in the site
2	Plot Label		Label of the plot in the site
3	ESU #		Number of the Elementary Sampling Unit (ESU)
4	ESU Label		Label of the ESU in the campaign
5	Northing Coord.		Geographical coordinate: Latitude (°), WGS-84
6	Easting Coord.		Geographical coordinate: Longitude (°), WGS-84
7	Extent (m) of ESU (diameter)		Size of the ESU ⁽¹⁾
8	Land Cover		Detailed land cover
9	Start Date (dd/mm/yyyy)		Starting date of measurements
10	End Date (dd/mm/yyyy)		Ending date of measurements
11	Products*	Method	Instrument
12		Nb. Replications	Number of Replications
13		Products*	Methodology
14		Uncertainty	Standard deviation

*LAI_{eff}, LAI, FAPAR and FCOVER

Ancillary data (Crop information, reflectance, aerosol optical depth) is provided in separated files (/field data/ancillary/).

Figure 10 to Figure 12 show the measurements obtained during the field experiment per land cover type and per ESU.

LAI_{eff} shows values ranging from 1.5 (Soybean) to 3 (Rice) (Figure 10). The LAI shows a similar distribution although with higher values due to the correction of the clumping. Maximum values are reported for Maize and lower for Soybean.

FAPAR daily integrated values are approximately around 0.8 (Figure 11), with minimum values for corn, and maximum for rice. Slightly lower results (0.39 and 0.36) were obtained for a pair of ESUS (#15 and #16) – Maize field.

For the FCOVER variable (Figure 12) a large variability than for FAPAR is observed, this could be partly explained due to the variability of shaded areas in the vertical direction is larger than at larger zenith angles.

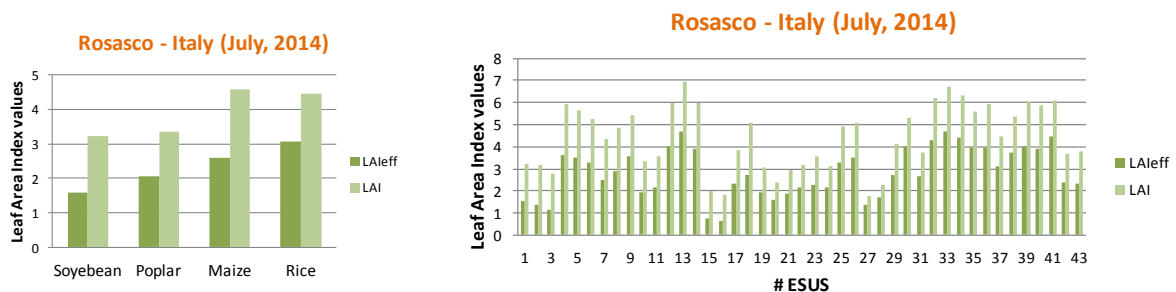


Figure 10: LAI_{eff} and LAI measurements acquired in Rosasco site, during the campaign of 3rd of July 2014. Left: Distribution by land cover type. Right: Distribution by ESUs.

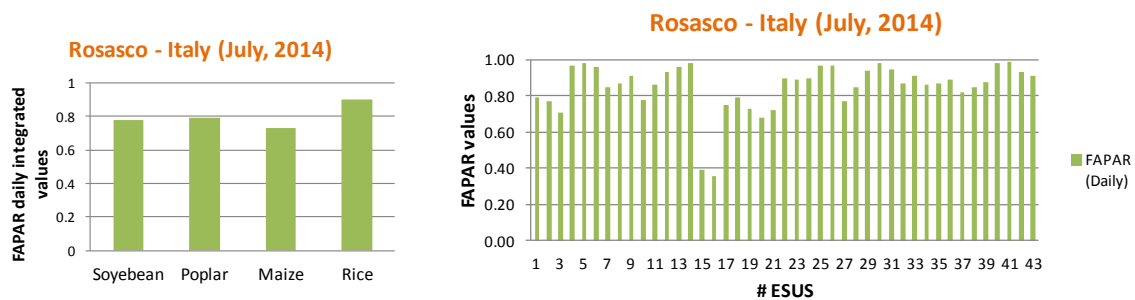


Figure 11: As in figure 10 for FAPAR (daily integrated values).

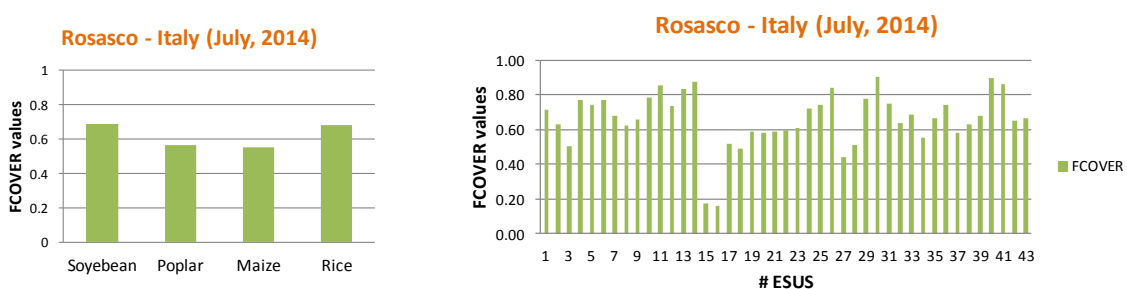


Figure 12: As in figure 10 for FCOVER.

Figure 13 shows the distribution of the measured variables, covering typically from medium to high values. For the FAPAR larger frequencies are observed around higher values, whereas for the FCOVER the larger frequencies are around 0.6.

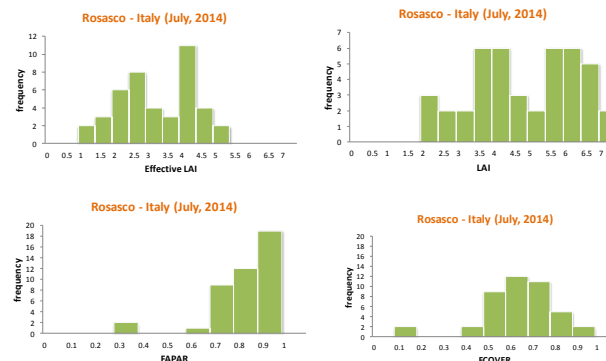


Figure 13: Distribution of the measured biophysical variables over the ESUs. Rosasco site, during the campaign of 3rd July, 2014.

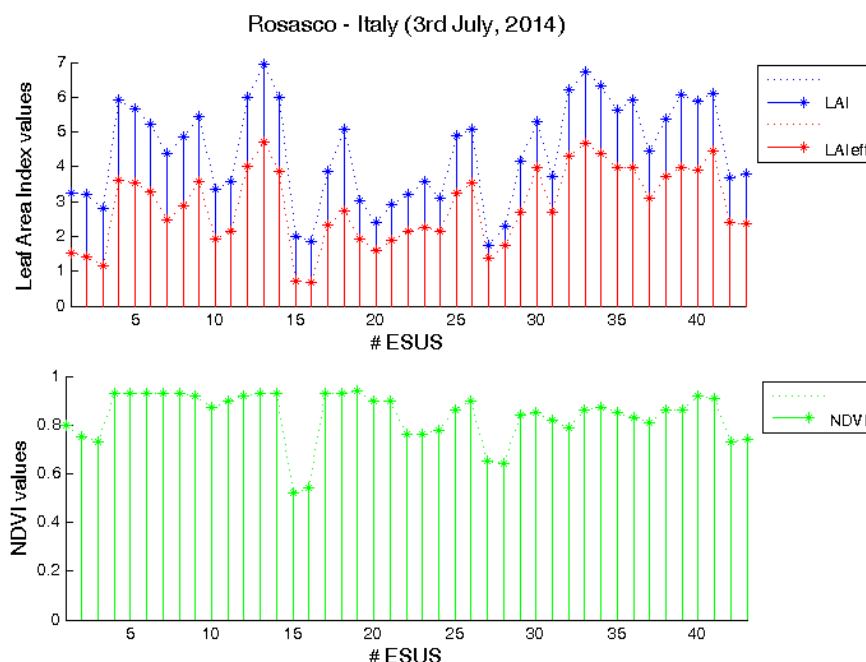


Figure 14: LAI (effective and actual) and NDVI measurements acquired in Rosasco site during the intensive field campaign 3rd July 2014, distributed by ESUs.

Figure 14 shows a comparison of the LAI and the NDVI values of the Landsat-8 image for the different ESUs. A consistent pattern can be observed for most of the ESUs, with highest (lowest) NDVI values where the highest (lowest) LAI values were measured. However, for some ESUs (e.g., from #5 to #15) the variability of LAI values is not well reproduced in the

NDVI, and the NDVI is saturated (around 0.9) for the LAI values larger than 4. This anticipates problems of the transfer function to reach the maximum ground LAI values from this Landsat-8 image. This problem will be partly solved by using other spectral bands, but will introduce a limitation in the information contained in the NIR band.

4.3.3. Ancillary information

- **Atmospheric characteristics**

Photometric measurements were taken the 3rd of July in a location within the study area from the 11:20 am to 12:50 pm using the EKO MS-120 sunphotometer. Resulting $\tau_{550} = 0.243$

(ImagineS_ESUdescription_Ancillary_Atmosphere.xls)

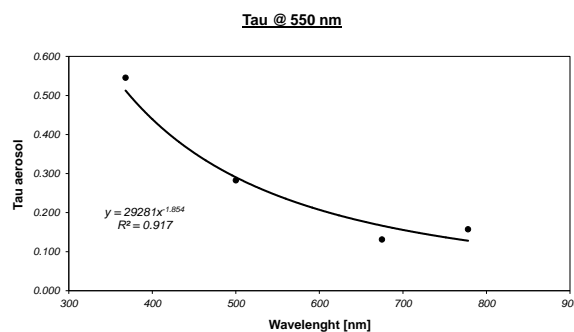


Figure 15: Aerosol Optical Depth (AOD) estimation for 550 nm wavelength

- **Crop information**

Some measurements of plant characteristics have been taken in contemporary with hemispherical photos, among which plant height, leaf length, flood presence etc. The file (ImagineS_ESUdescription_Ancillary_CropInfo.xls) reports these data together with agronomical information for each fields such as the cultivar and the sowing date.

- **Radiometric measurements**

Radiometric measurements were taken using the ASD Field Spec FR the 3rd of July near the satellite Landsat-8 overpass.

The attached file (ImagineS_ESUdescription_Ancillary_FieldSpect.xlsx) reports the sampling scheme ("SamplingScheme" sheet) and the measured reflectance spectra on corn ("mais30" and "mais29" sheets), soybean ("soybean28" sheet) and rice ("rice321" sheet). In two cases, soybean28 and mais30, the GPS coordinates are referred to the centroid of the field, therefore are the same for all the spectra.

5. EVALUATION OF THE SAMPLING

5.1. EVALUATION BASED ON NDVI VALUES

The sampling strategy is evaluated using the Landsat-8 TOC image by comparing the NDVI distribution over the site with the NDVI distribution over the ESUs (Figure 16). As the number of pixels is drastically different for the ESU and whole site (WS) it is not statistically consistent to directly compare the two NDVI histograms. Therefore, the proposed technique consists in comparing the NDVI cumulative frequency of the two distributions by a Monte-Carlo procedure which aims at comparing the actual frequency to randomly shifted sampling patterns. It consists in:

1. computing the cumulative frequency of the N pixel NDVI that correspond to the exact ESU locations; then, applying a unique random translation to the sampling design (modulo the size of the image)
2. computing the cumulative frequency of NDVI on the randomly shifted sampling design
3. repeating steps 2 and 3, 199 times with 199 different random translation vectors.

This provides a total population of $N = 199 + 1$ (actual) cumulative frequency on which a statistical test at acceptance probability $1 - \alpha = 95\%$ is applied: for a given NDVI level, if the actual ESU density function is between two limits defined by the $N\alpha / 2 = 5$ highest and lowest values of the 200 cumulative frequencies, the hypothesis assuming that WS and ESU NDVI distributions are equivalent is accepted, otherwise it is rejected.

Figure 16 shows that the NDVI distribution of Rosasco – July, 2014 campaign is good over the whole site (comprised between the highest and lowest cumulative frequencies). The sampling presents a bias towards higher vegetation values.

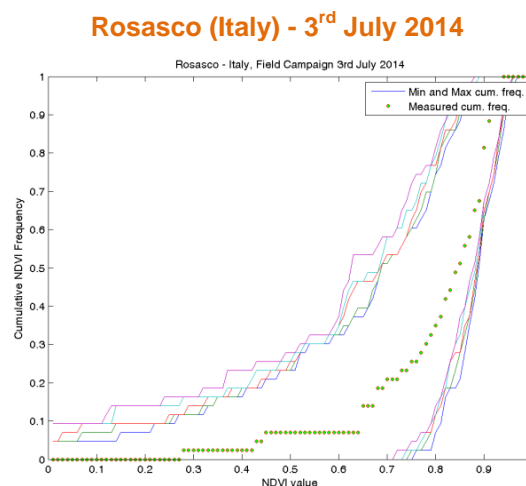


Figure 16: Comparison of NDVI distribution between ESUs and over the whole image. Field campaign (3rd July, 2014), Rosasco site (Italy).

5.2. EVALUATION BASED ON CONVEX HULL: PRODUCT QUALITY FLAG.

The interpolation capabilities of the empirical transfer function used for up-scaling the ground data using decametric images is dependent of the sampling (Martinez et al., 2009). A test based on the convex hulls was also carried out to characterize the representativeness of ESUs and the reliability of the empirical transfer function using the different combinations of the selected bands of the Landsat-8 TOC image. Two flag images are computed over the TOC reflectances, one for each band combination used for generating the empirical biophysical maps: SWIR-NIR-Red-Green (SNRG) was selected for FAPAR and FCover, whereas SWIR-NIR (SN) was used for LAI (see Section 6.2 for details). The result on convex-hulls can be interpreted as:

- pixels inside the 'strict convex-hull': a convex-hull is computed using all the Landsat-8 TOC reflectances corresponding to the ESUs belonging to the class. These pixels are well represented by the ground sampling and therefore, when applying a transfer function the degree of confidence in the results will be quite high, since the transfer function will be used as an interpolator;
- pixels inside the 'large convex-hull': a convex-hull is computed using all the reflectance combinations ($\pm 5\%$ in relative value) corresponding to the ESUs. For these pixels, the degree of confidence in the obtained results will be quite good, since the transfer function is used as an extrapolator (but not far from interpolator);
- pixels outside the two convex-hulls: this means that for these pixels, the transfer function will behave as an extrapolator which makes the results less reliable. However, having a priori information on the site may help to evaluate the extrapolation capacities of the transfer function.

Table 55: Percentages over the two areas over the test site of Rosasco (Italy).Convex hull values: 0=extrapolation of TF, 1=strict convex hull and 2=large convex hull).

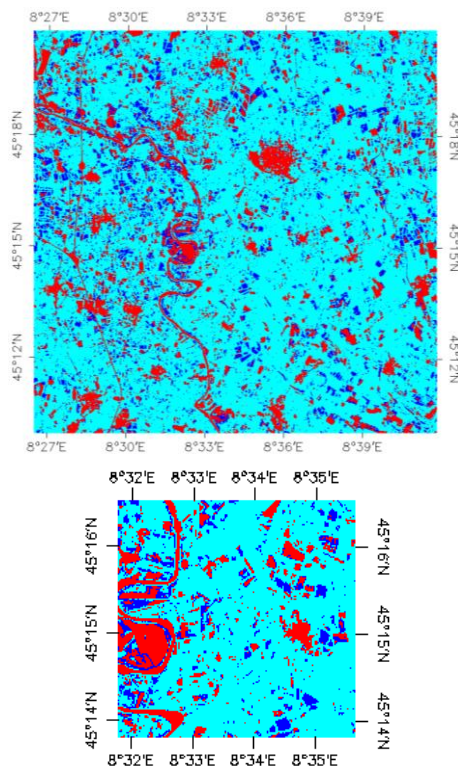
Field Campaign		Quality Flags (%)				
DATE	3 rd July, 2014					
SNRG	20x20 km ²			5x5 km ²		
Convex hull values	0	1	2	0	1	2
	14%	76%	10%	12%	80%	8%
SN	20x20 km ²			5x5 km ²		
Convex hull values	0	1	2	0	1	2
	7%	88%	5%	6%	90%	4%

Figure 17 shows the results of the Convex-Hull test (i.e., Quality Flag images) for the Rosasco site over the 5x5 km² study area and the extended 20x20 km² area. The strict and

large convex-hulls are high around the test site for the largest zone, 86% and 93% for the SNRG and SN combination, respectively. For the study area ($5 \times 5 \text{ km}^2$), the percentage of good interpolation confidence of the transfer function goes up to 88% and 94%, respectively (Table 5). Note that the pixels flagged as of lower quality (i.e. where the transfer function behaves as extrapolator) correspond in most cases to urban or water areas.

Rosasco site – Italy 3rd July, 2014

SWIR – NIR – RED – GREEN combination



SWIR – NIR combination

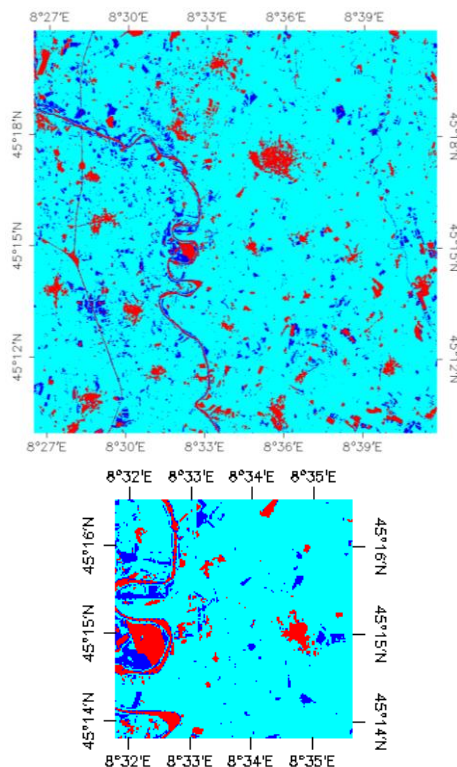


Figure 17: Convex Hull test over $20 \times 20 \text{ km}^2$ and $5 \times 5 \text{ km}^2$ areas. Left side: SNRG combination. Right side: SN combination. Clear and dark blue correspond to the pixels belonging to the 'strict' and 'large' convex hulls. Red corresponds to the pixels for which the transfer function behaves as extrapolator. Rosasco - Italy, 3rd July 2014.

6. PRODUCTION OF GROUND-BASED MAPS

6.1. IMAGERY

The Landsat-8/OLI images were acquired the 3rd July 2014 (overpass time 10:10 SLT) by OLI sensor (see Table 6 for acquisition properties). Four spectral bands were selected from 500 nm to 1750 nm with a nadir ground sampling distance of 30 m. The image was atmospherically corrected using ATCOR (Atmospheric Correction and Haze Reduction) tool (see 4.3.3) Therefore, for the transfer function analysis, the input satellite data used is Top of Canopy (TOC) reflectance. The original projection is UTM 32 North, WGS-84.

Table 6: Acquisition properties of Landsat-8 data used for retrieving high resolution maps.

Landsat- 8 TOA METADATA	
Platform / Instrument	Landsat- 8 / OLI_TIRS
Path	194
Row	29
Spectral Range	B3(green) : 0.53-0.59 μm B4(red) : 0.64-0.67 μm B5(NIR) : 0.85-0.88 μm B6(SWIR1) : 1.58-1.65 μm
3 rd July 2014 campaign	
Acquisition date	2014-07-03 10:10:55
Illumination Azimuth angle	136.328°
Illumination Elevation angle	63.059°
Ground Control Points	119
Geometric RMSE	3.307

6.2. THE TRANSFER FUNCTION

6.2.1. The regression method

If the number of ESUs is enough, multiple robust regression 'REG' between ESUs reflectance and the considered biophysical variable can be applied (Martínez et al., 2009): we used the 'robustfit' function from the Matlab statistics toolbox. It uses an iteratively re-weighted least squares algorithm, with the weights at each iteration computed by applying the bi-square function to the residuals from the previous iteration. This algorithm provides lower weight to ESUs that do not fit well.

The results are less sensitive to outliers in the data as compared with ordinary least squares regression. At the end of the processing, two errors are computed: weighted RMSE

(RW) (using the weights attributed to each ESU) and cross-validation RMSE (RC) (leave-one-out method).

As the method has limited extrapolation capacities, a flag image for each transfer function (Figure 17), are included in the ground based maps in order to inform the users on the reliability of the estimates. This information is very important to remove water or urban areas.

6.2.2. Band combination

Figure 18 shows the errors (RW, RC) obtained for the several band combinations using TOC reflectance. Attending specifications of lower cross-validation RMSE (RC) and weighted RMSE (RW) and the low number of rejected points, the selected band combination for FAPAR and FCOVER variables is: band 1 (green), band 2 (red), band 3 (Near Infrared) and band 4 (Short Wave Infrared) combination (SNRG).

Rosasco site – Italy 3rd July, 2014

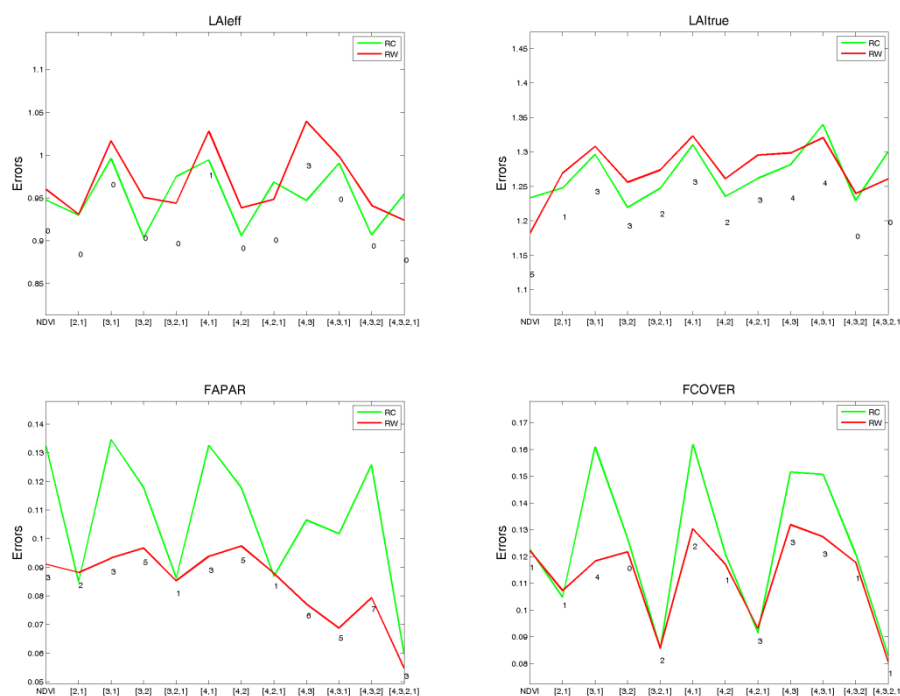


Figure 18: Test of multiple regression (TF) applied on different band combinations. Band combinations are given in abscissa (1=G, 2=RED, 3=NIR and 4=SWIR). The weighted root mean square error (RMSE) is presented in red along with the cross-validation RMSE in green. The numbers indicate the number of data used for the robust regression with a weight lower than 0.7 that could be considered as outliers.

For the LAI and LAIeff variables the selected combination was band 3 (Near Infrared) and band 4 (Short Wave Infrared) even if other combinations presented less errors or rejected points. This combination presented less saturation and slightly better linear response with

ground data. Moreover the dynamic range of the retrieved variable was more in agreement with the ground data than other combinations which provide much lower values.

6.2.3. The selected Transfer Function

The applied transfer function is detailed in Table 7, along with its weighted and cross validated errors.

Table 7: Transfer function applied to the whole site for LAleff, LAI, FAPAR daily integrated and FCOVER. RW for weighted RMSE, and RC for cross-validation RMSE.

Variable	Band Combination	RW	RC
First Campaign			
LAleff	$2.8462547 - 0.00221798 \cdot (\text{SWIR}) + 0.00129369 \cdot (\text{NIR})$	1.039	0.866
LAI	$3.6191378 - 0.00256012 \cdot (\text{SWIR}) + 0.00173978 \cdot (\text{NIR})$	1.298	1.201
FAPAR daily integrated	$0.50874225 - 0.00047540 \cdot (\text{SWIR}) - 0.00086665 \cdot (\text{R}) + 0.00028411 \cdot (\text{NIR}) + 0.00117861 \cdot (\text{G})$	0.097	0.055
FCOVER	$0.21931318 - 0.00022993 \cdot (\text{SWIR}) - 0.00121285 \cdot (\text{R}) + 0.00019589 \cdot (\text{NIR}) + 0.00118834 \cdot (\text{G})$	0.080	0.077

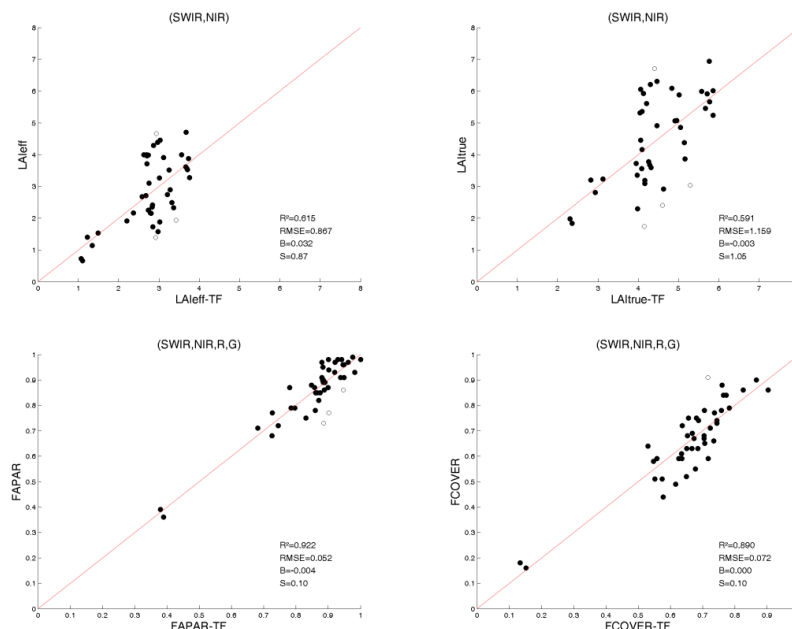


Figure 19: LAleff, LAI, FAPAR and FCOVER results for regression on reflectance using 2 and 4 bands combination. Full dots: Weight>0.7. Empty dots: 0<Weight<0.7 crosses.

Figure 19 shows scatter-plots between ground observations and their corresponding transfer function (TF) estimates for the selected bands combinations. A good correlation is

observed for the FAPAR and FCOVER with points distributed along the 1:1 line and no bias, and small scattering. However, for the LAI and LAI_{eff}, the transfer function estimates displays quite large dispersion for high values (RMSE is 1.2 for LAI). As reported previously, the NDVI provides very similar values for the highest LAI ground estimates in several ESUs. The transfer function tends to smooth the variability, providing no mean bias for the selected ESUs. Nevertheless, the mean values over the study area could be underestimated if the ESUs with largest LAI values are dominant in the study area.

6.3. THE HIGH RESOLUTION GROUND BASED MAPS

The high resolution maps are obtained applying the selected transfer function (Table 7) to the Landsat-8 TOC reflectance. Figures 20, 21 and 22 present the TF biophysical maps over the extended 20x20 km² area. Figure 17 shows the Quality Flags included in the final product.

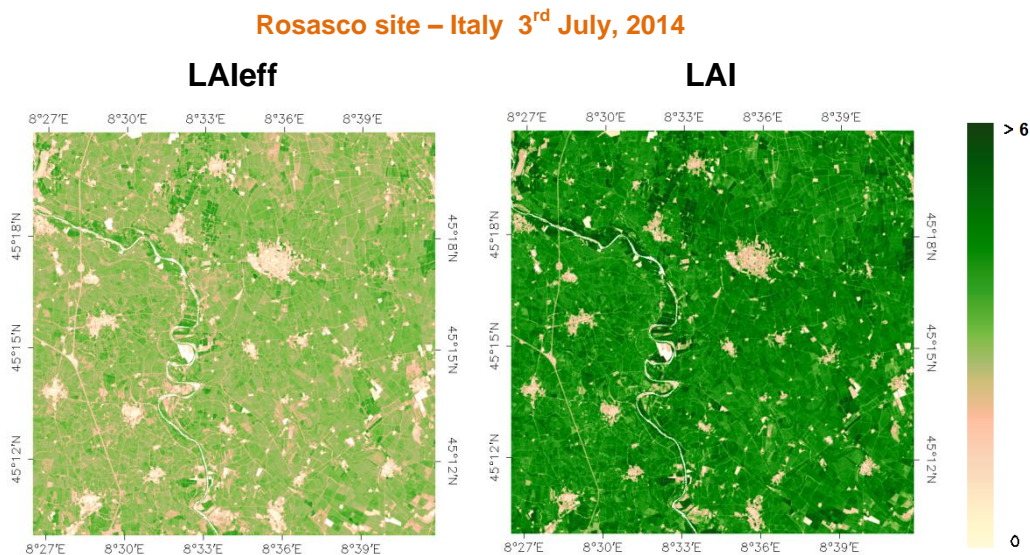


Figure 20: Ground-based LAI maps (20x20 km²) retrieved on the Rosasco site (Italy), 3rd July 2014. Left: LAI_{eff}. Right: LAI.

The best combination of bands obtained for LAI_{eff} and LAI is SWIR and NIR bands, however the river and some urban areas are overestimated, its quality flag recognizes these zones with zero value.

Rosasco site – Italy 3rd July, 2014

FAPAR daily integrated

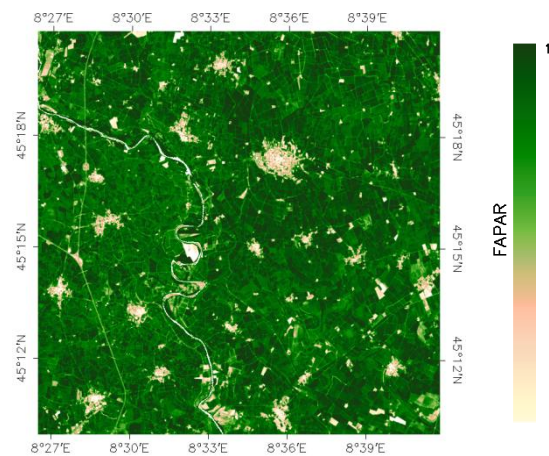


Figure 21: Ground-based FAPAR maps (20x20 km²) retrieved on the Rosasco site (Italy), 3rd July 2014.

Rosasco site – Italy 3rd July, 2014

FCOVER

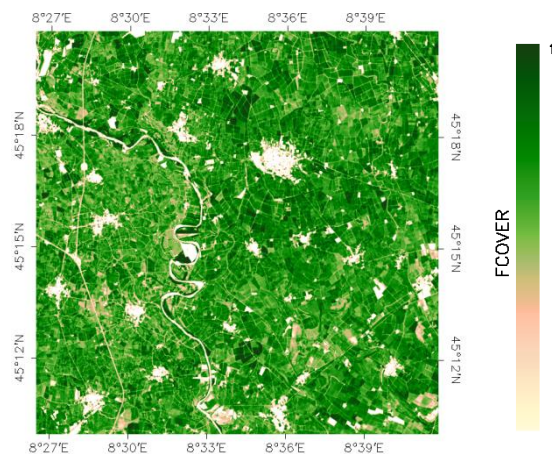


Figure 22: Ground-based FCOVER map (20x20 km²) retrieved on the Rosasco site (Italy), 3rd July 2014.

Figure 23 shows these ground-based high resolution maps over the 5x5 km² study area. These maps are provided for validation of satellite products at different spatial resolutions.

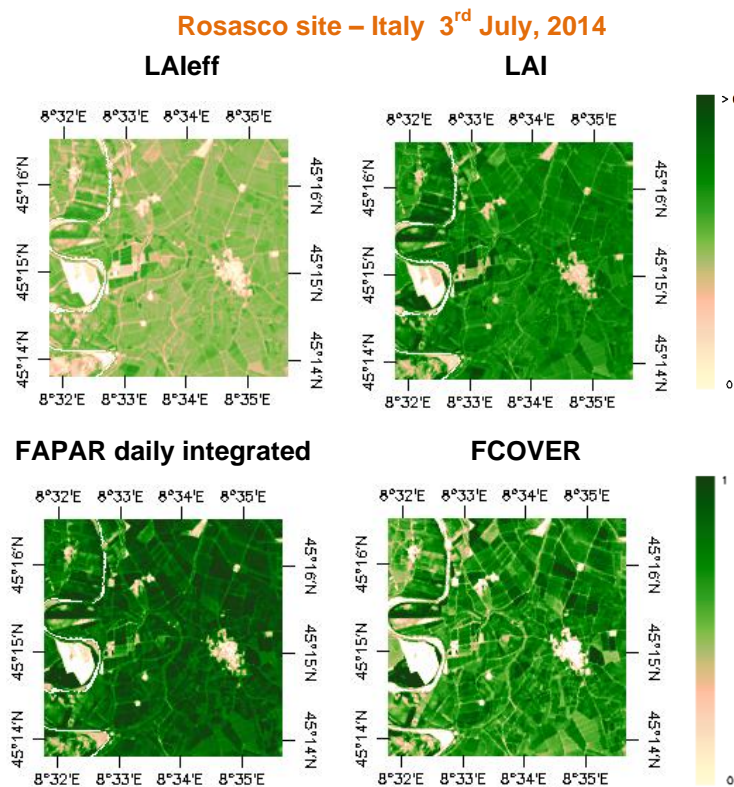


Figure 23: Ground-based maps (5x5 km²) retrieved on the Rosasco site (Italy), 3rd July 2014.

6.3.1. Mean Values

Mean values of a 3x3 km² area centred in the test site are provided for validation of 1 km satellite products to reduce co-registration and PSF errors, and in agreement with the CEOS OLIVE direct dataset (Table 8). For the validation of coarser resolutions product (e.g. MSG products) a larger area should be considered. For this reason empirical maps are provided at 5x5 km², and 20x20 km².

Table 8: Mean values and standard deviation (STD) of the HR biophysical maps for the selected 3 x 3 km² area at Rosasco site (Italy).

Rosasco - 3x3 km ²		LATITUDE	LONGITUDE
		45.253 N	8.562 E
LAI _{eff}	MEAN	2.62	
	STD	0.59	
LAI	MEAN	4.20	
	STD	0.76	
FAPAR daily	MEAN	0.85	
	STD	0.17	
FCOVER	MEAN	0.67	
	STD	0.19	

Table 9 describes the content of the geo-biophysical maps in the nomenclature: "BIO_YYYYMMDD_SENSOR_Site ETF_Area" files, where:

BIO stands for Biophysical (LAI_{eff}, LAI, FAPAR and FCOVER)

SENSOR = LANDSAT8

YYYYMMDD = Campaign date

Site = Rosasco

ETF stands for Empirical Transfer Function

Area = window size 20x20 km² and 5x5 km²

Table 9: Content of the dataset.

Parameter	Dataset name	Range	Variable Type	Scale Factor	No Value
LAI effective	LAI _{eff}	[0, 7]	Integer	1000	-1
LAI	LAI	[0, 7]	Integer	1000	-1
FAPAR daily integrated	FAPAR	[0, 1]	Integer	10000	-1
Fraction of Vegetation Cover	FCOVER	[0, 1]	Integer	10000	-1
Quality Flag	QFlag	0,1,2 (*)	Integer	N/A	-1

(*) 0 means extrapolated value (low confidence), 1 strict interpolator (best confidence), 2 large interpolator (medium confidence)

7. CONCLUSIONS

The FP7 ImagineS project continues the innovation and development activities to support the operations of the Copernicus Global Land service. One of the ImagineS demonstration sites, a rice site of the ERMES project, is located near Rosasco, in the Province of Pavia, in the Italian region Lombardy. This site is between the Sesia river and the city of Rosasco.

This report first presents the ground data collected during an intensive field campaign on 3rd of July of 2014. The dataset includes 43 elementary sampling units where digital hemispherical photographs were taken and processed with the CAN-EYE software to provide LAI, LAI_{eff}, FAPAR and FCOVER values to characterize the natural vegetation of the area (cultivated) as well as a Poplar tree plantation in the study area. Standard digital photos, plant height and phenological stage were also taken to “characterize” the fields. Additional reflectance measurements were taken in 5 fields (Rice and Corn). Sunphotometer measurements for atmospheric correction were taken using an EKO sunphotometer with 5 spectral channels.

High resolution ground-based maps of the biophysical variables were produced over the site. Ground-based maps have been derived using high resolution imagery (Landsat-8 TOC reflectance) according with the CEOS LPV recommendations for validation of low resolution satellite sensors. Transfer functions have been derived by multiple robust regressions between ESUs reflectance and the several biophysical variables. The spectral band combinations to minimize errors (weighted RMSE and cross-validation RMSE) were band 1 (green), band 2 (red), band 3 (Near Infrared) and band 4 (Short Wave Infrared) for FAPAR and FCOVER variables, whereas band 3 (Near Infrared) and band 4 (Short Wave Infrared) for LAI_{eff} and LAI variables. The RMSE values for the several transfer function estimates are 0.87 for LAI_{eff}, 1.16 for LAI, 0.05 for daily integrated FAPAR, and finally 0.07 for FCOVER, with no bias and low scattering for FAPAR and FCOVER. For the LAI, the transfer function tends to smooth the ground variability, and the mean values for validation should be used with caution (possible underestimation of LAI)

The quality flag maps based on the convex-hull analysis show a very good quality around the study area. The percentages for the FAPAR/FCover and LAI transfer function of good interpolation capabilities for the 5x5 km² study area are 88% and 94% respectively. The urban and water areas are well identified in the quality flag maps.

The biophysical variable maps are available in geographic (UTM 32 North projection WGS-84) coordinates at 30 m resolution over the 20x20 km² and 5x5 km² over the site. Mean values and standard deviation over a validation area of 3x3 km² for LAI_{eff}, LAI, FCOVER and FAPAR were computed centered at the validation test site.

8. ACKNOWLEDGEMENTS

This study is supported by the FP7 IMAGINES project under Grant Agreement N°311766, and for the FP7 ERMES project under Grant Agreement N° 606983. Landsat 8-HR imagery is provided through the USGS Global Visualization service. Thanks to the CNR-IREA for providing ground dataset and the TOC reflectance data.

9. REFERENCES

- Baret, F. and Fernandes, R. (2012). Validation Concept. VALSE2-PR-014-INRA, 42 pp.
- Camacho, F., Cernicharo, J., Lacaze, R., Baret, F., and Weiss, M. (2013). GEOV1: LAI, FAPAR Essential Climate Variables and FCOVER global time series capitalizing over existing products. Part 2: Validation and intercomparison with reference products. *Remote Sensing of Environment*, 137: 310-329.
- Demarez, V., Duthoit, S., Baret, F., Weiss, M. and Dedieu, G. (2008). Estimation of leaf area and clumping indexes of crops with hemispherical photographs. *Agricultural and Forest Meteorology*, 148, 644-655.
- Fernandes, R., Plummer, S., Nightingale, J., et al. (2014). Global Leaf Area Index Product Validation Good Practices. CEOS Working Group on Calibration and Validation - Land Product Validation Sub-Group. *Version 2.0.1: Public version made available on LPV website*.
- Martínez, B., García-Haro, F. J., & Camacho, F. (2009). Derivation of high-resolution leaf area index maps in support of validation activities: Application to the cropland Barrax site. *Agricultural and Forest Meteorology*, 149, 130–145.
- Miller, J.B. (1967). A formula for average foliage density. *Aust. J. Bot.*, 15:141-144
- Morissette, J. T., Baret, F., Privette, J. L., Myneni, R. B., Nickeson, J. E., Garrigues, S., et al. (2006). Validation of global moderate-resolution LAI products: A framework proposed within the CEOS land product validation subgroup. *IEEE Transactions on Geoscience and Remote Sensing*, 44, 1804–1817.
- Latorre, C., Camacho, F., Pérez, Beget M.E. and Di Bella, C. (2014). "Vegetation Field Data and Production of Ground-Based Maps: 25 de Mayo site. La Pampa, ARGENTINA" report. 18 -20 (Available at ImagineS website: <http://fp7-imagines.eu/pages/documents.php>).
- Weiss, M., Baret, F., Smith, G.J., Jonckheere, I. and Coppin, P., (2004). Review of methods for in situ leaf area index (LAI) determination. Part II. Estimation of LAI, errors and sampling. *Agricultural and Forest Meteorology*, 121, 37–53.
- Weiss M. and Baret F. (2010). CAN-EYE V6.1 User Manual
- Welles, J.M. and Norman, J.M., 1991. Instrument for indirect measurement of canopy architecture. *Agronomy J.*, 83(5): 818-825.